

Semimicroscopic analysis of ${}^6\text{Li}$ elastic scattering at 40 MeV/nucleon

M. Anwar ^{*}*Department of Physics, Faculty of Science, Aswan University, Aswan 81528, Egypt*

(Received 21 March 2020; accepted 1 June 2020; published 18 June 2020)

Analysis of the differential cross sections for ${}^6\text{Li}$ elastic scattering from ${}^{24}\text{Mg}$, ${}^{28}\text{Si}$, ${}^{40}\text{Ca}$, ${}^{48}\text{Ca}$, ${}^{58}\text{Ni}$, ${}^{90}\text{Zr}$, and ${}^{116}\text{Sn}$ at 40 MeV/nucleon is performed within the framework of the optical double folding model. Simple phenomenological effective nucleon-nucleon interaction represented by a density-independent single Yukawa term is utilized to generate the real optical potential part. The derived potentials in conjunction with imaginary parts expressed in phenomenological volume Woods-Saxon forms have been successfully used to reproduce the seven sets of data. For the sake of comparison, the same measurements are reanalyzed using folded potentials based upon the density-independent M3Y effective interaction. Furthermore, reasonably successful reproduction of the data is obtained by Woods-Saxon-type optical model potentials. The radial sensitivity of the derived real potentials to the calculating elastic-scattering angular distributions has been investigated using the notch perturbation technique. The target mass dependence in real and imaginary volume integrals as well as total reaction cross sections are also investigated.

DOI: [10.1103/PhysRevC.101.064617](https://doi.org/10.1103/PhysRevC.101.064617)

I. INTRODUCTION

The optical model (OM) is useful for describing the interaction of nuclear particles involved in elastic scattering as well as in more complicated processes. The complex potential of the OM considers the many open channels by including an imaginary part representing the loss of flux from the channel in consideration. Elastic scattering is the simplest process that occurs in a heavy-ion (HI) collision because it involves very little rearrangement of matter and energy. Therefore, this process has been studied in many experimental investigations, and a huge body of elastic cross-section data is currently available.

The double folding (DF) model is one of the simplest and most appropriate tools for constructing the interaction potential between complex nuclei. In the DF model, a realistic effective nucleon-nucleon (NN) interaction is folded over the distributions of nucleons within the projectile and target nuclei. One of the most famous and successful effective NN interactions is the so-called M3Y G -matrix interaction [1] or its density-dependent version [2,3]. The DF potentials with these versions usually provide only the real part of the nucleus-nucleus potential. In this case, the imaginary potential added to the real DF potential is commonly represented in the Woods-Saxon (WS) form or its derivative. Accordingly, the potential parameters included are determined phenomenologically to reproduce the experimental data of elastic scattering.

During several decades, it has been reported that the breakup of the weakly bound ${}^6\text{Li}$ projectile is responsible for the reduction in the renormalization factor ($N_R \approx 0.5$ to 0.6) of the folded potential. This drop is necessary to fit

elastic-scattering data. This effect could be simulated by a complex dynamic polarization potential (DPP). The real DPP part is added as a repulsive term at nuclear potential surface. Sakuragi *et al.* [4], Sakuragi [5], and Sakuragi *et al.* [6] applied coupled discretized continuum channel (CDCC) techniques to confirm that the elastic-scattering data can be fitted well with the potential renormalization close to unity when coupling to break up the channel is included. They reported that elastic HI scattering is almost insensitive to the potential at the nuclear interior due to a strong absorptive potential except for a few cases of high-energy scattering. In the case of high energies, cross sections at large angles are very sensitive to the details of the potential at the nuclear interior since the observed large angle scattering displays nuclear rainbowlike enhancements. Also, Pang and Mackintosh [7] studied the DPP due to the breakup of the projectile for ${}^6\text{Li}$ scattering from ${}^{12}\text{C}$ at five laboratory energies from 90 to 318 MeV. They determined the DPP by calculating the potential that exactly reproduces the S matrix when the process of the breakup is included in CDCC calculations. An extensive discussion of this method that is far away from our interest is presented in Ref. [8]. On the other hand, the assumption that the breakup effects strongly contribute to the DPP only at the surface region is well established [9,10].

It is worth noting that the elastic scattering of ${}^6\text{Li}$ supplies a strong test of the validity for HI potential models [11]. Large bodies of data have been accumulated in the case of ${}^6\text{Li}$ scattering on various targets. The elastic scattering of ${}^6\text{Li}$ with several targets has been extensively studied below 200 MeV [12–18]. Nadasen and co-workers [19,20] have studied ${}^6\text{Li}$ elastic scattering from ${}^{12}\text{C}$, ${}^{28}\text{Si}$, ${}^{40}\text{Ca}$, ${}^{58}\text{Ni}$, ${}^{90}\text{Zr}$, and ${}^{208}\text{Pb}$ at 210 MeV only with WS potentials and from ${}^{12}\text{C}$ and ${}^{28}\text{Si}$ at 318 MeV with phenomenological and folding OM potentials [21]. A study of 600-MeV ${}^6\text{Li}$ scattering on

^{*} melfawy99@aswu.edu.eg

^{12}C , ^{58}Ni , ^{90}Zr , and ^{208}Pb targets was performed, and the coupling effect between the elastic and the breakup channels at an intermediate energy was reported in Ref. [22]. Farid and Hassanain [11,23] have analyzed 73–318 MeV ^6Li elastic and inelastic scatterings from ^{12}C , ^{28}Si , ^{40}Ca , ^{58}Ni , ^{90}Zr , and ^{208}Pb using DFM calculations with density-independent M3Y and Jeukenne-Lejeune-Mahaux (JLM) effective NN interactions.

To extract a systematic optical potential (OP) for loosely bound nuclei, Trache *et al.* [24] and Carstoiu *et al.* [25] have obtained OM parameters from the fits to the elastic-scattering angular distributions using the density-dependent JLM effective NN interaction in DF calculations. They suggested that one can, indeed, obtain the OM potentials for pairs of projectile-target nuclei for data which are not available or scarce by using a folding model procedure with renormalization factors extracted from the systematics. Also, Furumoto and Sakuragi [26] used the DF model with the JLM effective NN interaction for a systematic analysis of α -nucleus elastic scattering in the range of 40–240 MeV.

About 10 yr ago, elastic-scattering cross sections at 240 MeV of ^6Li particles from ^{24}Mg and ^{28}Si [27], ^{40}Ca and ^{48}Ca [28], ^{58}Ni and ^{90}Zr [29], and ^{116}Sn [30] were measured. The OP parameters were obtained for all reactions from the fit of elastic-scattering data using the DF model with other density-dependent M3Y effective NN interactions as well as the WS potential except for $^6\text{Li} + ^{24}\text{Mg}$ and $^6\text{Li} + ^{28}\text{Si}$ scattering systems which were obtained by fitting elastic scattering with two different DF potentials as well as WS potentials. The key for analyzing the interactions in Refs. [27–30] is the so-called scaling factor S_r on the radius of the calculated real OP. They argued that it represents the repulsive surface correction of DPP that is vital for a realistic description by the folding model.

On the other hand, based upon the α -cluster structure, several studies have been carried out to investigate the DF cluster potentials for the analyses of HI's elastic scattering [31–33]. Recently, six sets of $^6\text{Li} + ^{28}\text{Si}$ elastic-scattering data over the 76–318-MeV energy range have been analyzed using the α -cluster folding formalism [34]. Alternatively, the energy-density functional theory [35,36] is used to calculate the real part of the nucleus-nucleus potential to analyze the $^6\text{Li} + ^{28}\text{Si}$ reaction at $E_{\text{Lab}} = 7.5\text{--}318$ MeV, and it was compared with WS and squared WS forms.

Substantially, in the framework of the optical folding model, many theoretical investigations were performed for elastic scattering of heavy ions by a weakly bound nucleus as the ^6Li projectile [4–6,9–11,23–25]. One of the main motivations for these studies was related to the role of the ^6Li breakup and other reaction channels into a nuclear collision process in terms of the DPP. If, in these studies, the DPP influences are included, excellent results are obtained. In light of this context, my main motivation for the present paper is to simplify the calculation of the nuclear potential, in conjunction with obtaining the best fit with experimental data through twofold: (i) Study the effect of varying the ^6Li nuclear density distribution forms to select the simplest one which produces the best fit of the experimental data, and (ii) test the validity of using a simple NN interaction that could include the DPP effect.

The main goal of the present paper is analyzing the present data by DF calculations for the real part generated by simple density-independent single Yukawa (S1Y) effective NN interaction with a simple Gaussian form for the ^6Li projectile and without any external factor representing the effect of the DPP. For the sake of comparison, the same measurements have been analyzed using DF potentials based upon the density-independent M3Y effective interaction. Moreover, the notch test is employed to investigate the sensitivity of the elastic-scattering cross section to the various regions of the constructed real potentials.

In this paper, the elastic scattering of ^6Li on ^{24}Mg , ^{28}Si , ^{40}Ca , ^{48}Ca , ^{58}Ni , ^{90}Zr , and ^{116}Sn targets at 40 MeV/nucleon is analyzed. The phenomenological analyses of the elastic-scattering data are extracted in Sec. II. Section III specifies the details of the semimicroscopic real DF potentials generated based upon the S1Y and M3Y effective NN interactions with the fits to the elastic-scattering data. The final section is devoted to a summary of the results.

II. PHENOMENOLOGICAL ANALYSIS

The present elastic-scattering data have been analyzed with the program HIOPTIM-94 code [37] in a standard OM potential defined as

$$U(R) = V_C(R) - V_0 f_V(R) - iW_0 f_W(R), \quad (1)$$

where V_0 and W_0 are the depths of the real and imaginary parts of the potential with the WS form

$$f_x(R) = \left(1 + \exp\left\{\left[R - r_x(A_P^{1/3} + A_T^{1/3})\right]/a_x\right\}\right)^{-1} \quad \text{and} \\ x = V, W,$$

where r_x and a_x are the real (imaginary) radius parameter (in femtometers) and diffuseness of the potential (in femtometers), respectively. The Coulomb potential $V_C(R)$ for uniformly charge distributions [14,38] of the colliding nuclei with the radius $R_C = 1.4(A_P^{1/3} + A_T^{1/3})$ fm is used.

An automatic search is carried out in order to optimize the fits to data by minimizing the χ^2 which is defined

$$\chi^2 = \frac{1}{N} \sum_{i=1}^N \{[\sigma_{\text{cal}}(\theta_i) - \sigma_{\text{exp}}(\theta_i)]/\Delta\sigma(\theta_i)\}^2, \quad (2)$$

where N is the number of differential cross-section data points and $\sigma_{\text{cal}}(\theta_i)$ is the i th calculated cross section. $\sigma_{\text{exp}}(\theta_i)$ and $\Delta\sigma(\theta_i)$ are the corresponding experimental cross section and its relative uncertainty, respectively. The χ^2 values are obtained considering statistical errors for all analyzed data.

The theoretical predictions of the angular distribution of differential cross sections extracted using the WS phenomenological OP defined by Eq. (1) and dashed line are shown in Figs. 1 and 2 in comparison with the experimental data. All angular distributions display typical patterns for elastic scattering, dominated by strong absorption with Fraunhofer diffractive oscillations around the crossing point, followed by less developed structures at larger angles. The corresponding best-fit parameters extracted for all seven cases are listed in Table I. In addition to the depth, reduced radius, and diffuseness for the real and imaginary parts of the OP, the table gives

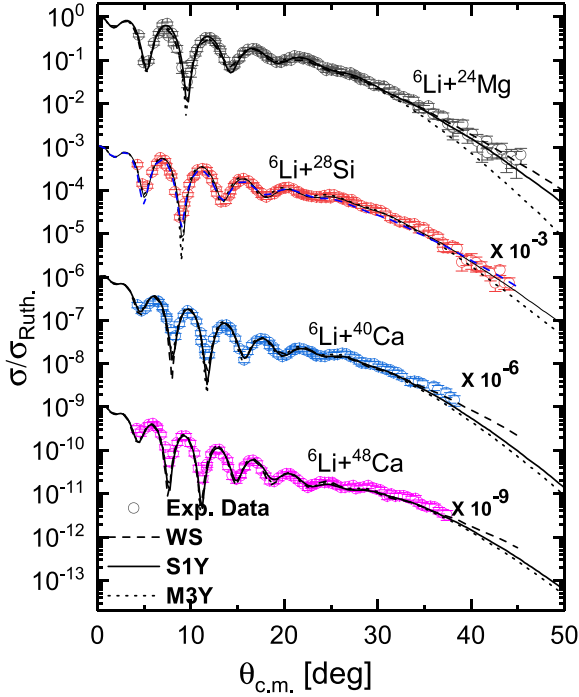


FIG. 1. Ratio of the elastic-scattering cross sections to the Rutherford cross section as a function of the scattering angles at $E_{\text{Lab}} = 240$ MeV for the ${}^6\text{Li}$ scattered from ${}^{24}\text{Mg}$, ${}^{28}\text{Si}$, ${}^{40}\text{Ca}$, and ${}^{48}\text{Ca}$. The dashed line denotes the calculated ratio generated by the phenomenological WS potentials of Eq. (1). The solid and dotted lines represent the results of the S1Y and M3Y semimicroscopic potentials, respectively.

the best-fit χ^2 , the total reaction cross-section (σ_R), the values of the volume integrals per pair of interacting nucleons for the real (J_R) and imaginary parts (J_I) of the potential, respectively, and, finally, the corresponding root-mean-square (rms) radii of the real $\langle r^2 \rangle_V^{1/2}$ and imaginary $\langle r^2 \rangle_W^{1/2}$ potentials. For the seven considered reactions, the data are well reproduced over all the measured angular ranges. These results are consistent with those extracted in previous studies [27–30]. It is noted that the radii of the imaginary potentials are about 20–30% larger than those of the real potentials.

III. FOLDING MODEL ANALYSIS

In addition to the analysis with WS-type potentials, the data have been reanalyzed in the framework of the semimicro-

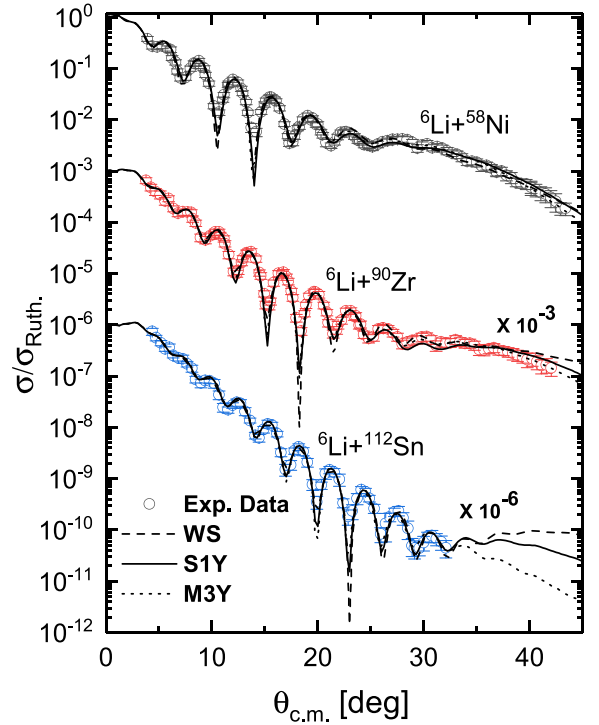


FIG. 2. The same as Fig. 1 but for the ${}^6\text{Li}$ scattered from ${}^{58}\text{Ni}$, ${}^{90}\text{Zr}$, and ${}^{116}\text{Sn}$ at $E_{\text{Lab}} = 240$ MeV.

scopic DF model. The nucleus-nucleus DF potential is given by

$$V_F(R) = \int \rho_1(\mathbf{r}_1)\rho_2(\mathbf{r}_2)v_{\text{NN}}(s)d\mathbf{r}_1d\mathbf{r}_2, \quad (3)$$

where ρ_1 and ρ_2 are nucleon densities in the projectile and target nuclei, respectively, R denotes the distance between the centers of mass of the colliding nuclei, $s = |\mathbf{R} + \mathbf{r}_1 - \mathbf{r}_2|$ is the relative vector between the interacting nucleon pair, and $v_{\text{NN}}(s)$ is the effective NN interaction used in the calculations.

Several effective NN interaction forms can be used for calculating the folding model potentials. In the present paper, two forms are considered. The first is the so-called S1Y interaction, a phenomenological density-independent single Yukawa term, which is defined as [39]

$$v_{\text{NN}}(s) = V_0 e^{-s/\mu} / (s/\mu), \quad (4)$$

TABLE I. WS phenomenological OP parameters obtained by fits of scattering data.

Interaction	V (MeV)	r_V (fm)	a_V (fm)	J_V (MeV) fm^3	$\langle r^2 \rangle_V^{1/2}$ (fm)	W (MeV)	r_W (fm)	a_W (fm)	J_W (MeV) fm^3	$\langle r^2 \rangle_W^{1/2}$ (fm)	σ_R (mb)	χ^2
${}^6\text{Li} + {}^{24}\text{Mg}$	114.58	0.757	0.891	243.35	4.31	34.63	0.963	1.031	141.30	5.19	1693	1.11
${}^6\text{Li} + {}^{28}\text{Si}$	143.34	0.720	0.944	262.82	4.43	32.13	1.016	0.921	129.16	5.13	1669	1.34
${}^6\text{Li} + {}^{40}\text{Ca}$	153.90	0.742	0.957	252.37	4.66	32.25	1.057	0.905	120.60	5.45	1918	1.86
${}^6\text{Li} + {}^{48}\text{Ca}$	153.10	0.788	0.893	251.94	4.70	32.00	1.084	0.823	114.32	5.5	1969	1.48
${}^6\text{Li} + {}^{58}\text{Ni}$	153.35	0.804	0.917	246.51	4.92	32.59	1.092	0.867	112.15	5.75	2179	1.76
${}^6\text{Li} + {}^{90}\text{Zr}$	159.61	0.889	0.799	261.24	5.26	38.61	1.089	0.979	116.08	6.44	2810	1.34
${}^6\text{Li} + {}^{116}\text{Sn}$	183.09	0.849	0.913	254.07	5.56	29.05	1.187	0.863	97.91	6.94	3014	0.99

with $V_0 \approx 60(1.0 - 0.005E/A_P)$ MeV, where E and A_P are the incident energy and the mass number of the projectile, respectively.

The most common M3Y Reid effective NN realistic interaction [3] is used as a second choice in the calculation. It has the form

$$v_{\text{NN}}(s) = 7999 \frac{e^{-4s}}{4s} - 2134.25 \frac{e^{-2.5s}}{2.5s} + J_{00}(E)\delta(s), \quad (5)$$

where $J_{00}(E)$ represents the single nucleon knock-on contribution to the interaction and is given by

$$J_{00}(E) = -276(1 - 0.005E/A_P). \quad (6)$$

Earlier, DF analyses [39] of HI elastic scattering at energies ($E/A_P \approx 10 - 100$ MeV/nucleon) are carried out by the S1Y interaction with a complex strength, suggested by Satchler [39] where experimental data for 36 sets of HI elastic scattering was successfully reproduced. The success of this NN interaction is restricted for peripheral HI scattering where the strong absorption is dominated. Satchler [39] and Satchler *et al.* [40] avoided light HI scattering systems where the elastic-scattering data are sensitive to the potential in the interior region at small radii. Farid and Hassanain tested the validity of the S1Y and M3Y effective interactions in analyzing the elastic scattering of a light HI [11,23] and the S1Y with JLM interactions for the $\alpha - \alpha$ system [41]. The DF model was employed to generate both the real and the imaginary potential parts for the former systems whereas the real part was calculated only for the later $\alpha - \alpha$ system.

Whereas the S1Y and M3Y effective interactions are used to deduce the real OP part, the imaginary part is treated phenomenologically using the WS potential in the three-parameter volume form as in Eq. (1).

Since the form of density distribution of colliding nuclei is crucial in DF calculations, four different matter density distributions for the loosely bound ${}^6\text{Li}$ ground state have been used enabling a comparative study.

(1) Fermi two parameters (F2P),

$$\rho(r) = \rho_0 \left[1 + \exp\left(\frac{r - 1.508}{0.5}\right) \right]^{-1}, \quad (7i)$$

with rms radius $\langle r^2 \rangle_m^{1/2} = 2.195$ fm as in Ref. [30].

(2) The form which has been constructed from a phenomenological electron-scattering proton charge distribution (PHN) with the assumption that the ${}^6\text{Li}$ proton and neutron densities are equal where $N = Z$ [11],

$$\begin{aligned} \rho(r) = & 0.203 \exp(-0.3306r^2) \\ & + [-0.0131 + 0.001378r^2] \\ & \times \exp(-0.1584r^2), \end{aligned} \quad (7ii)$$

with $\langle r^2 \rangle_m^{1/2} = 2.394$ fm.

(3) The form obtained from proton scattering with the cluster-orbital shell-model approximation (COSMA)

TABLE II. Parameters for the nuclear matter densities of the target's nuclei in form of the F2P model with its corresponding rms radius values.

Nucleus	ρ_0 (fm $^{-3}$)	c (fm)	a (fm)	$\langle r^2 \rangle^{1/2}$ (fm)	Reference
${}^{24}\text{Mg}$	0.17	2.995	0.478	2.922	[43]
${}^{28}\text{Si}$	0.175	3.15	0.475	3.012	[11]
${}^{40}\text{Ca}$	0.169	3.60	0.523	3.399	[11]
${}^{48}\text{Ca}$	0.187	3.723	0.515	3.479	[44]
${}^{58}\text{Ni}$	0.176	4.08	0.515	3.695	[45]
${}^{90}\text{Zr}$	0.165	4.90	0.515	4.251	[11]
${}^{116}\text{Sn}$	0.156	5.469	0.5	4.626	[30]

[30],

$$\begin{aligned} \rho(r) = & 2.0 \left(\frac{\exp[-r^2/(1.55)^2]}{\pi^{3/2}(1.55)^3} \right) \\ & + 1.0 \left(\frac{2 \exp[-r^2/(2.07)^2]}{3\pi^{3/2}(2.07)^5} \right) r^2, \end{aligned} \quad (7iii)$$

with $\langle r^2 \rangle_m^{1/2} = 2.444$ fm.

(4) Finally, in the form of a Gaussian [42] one term (GIT),

$$\rho(r) = \rho_0 \exp(-\beta r^2), \quad (7iv)$$

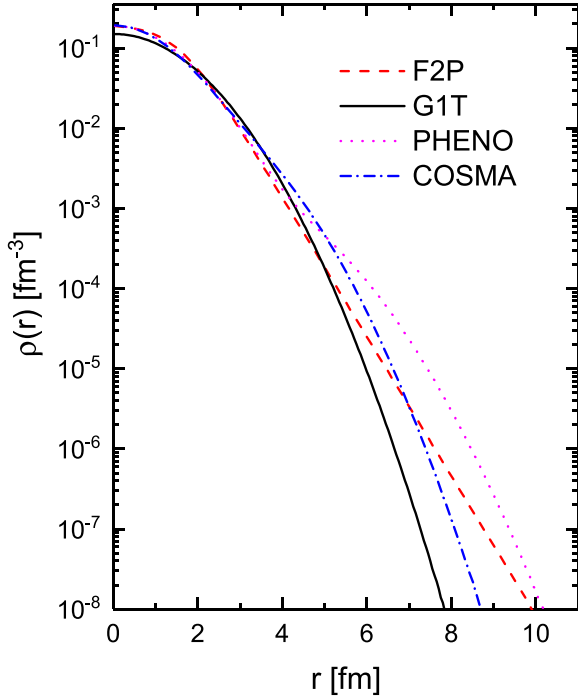
where β is adjusted to reproduce the recently rms radius value published in Ref. [46]. Here, $\langle r^2 \rangle_m^{1/2} = 2.36$ fm is used.

For all studied target densities, the F2P form defined by Eq. (7i) where the parameters ρ_0 , c (half density radius), and a (diffuseness) are shown in Table II with the corresponding $\langle r^2 \rangle_m^{1/2}$ values is used.

The four different densities of the ${}^6\text{Li}$ nucleus that have been used are displayed in Fig. 3. It shows that the PHN is the only density that produces a tail for ${}^6\text{Li}$ whereas the others are not. The rms radius of ${}^6\text{Li}$ is spread from 2.195 to 2.444 fm. In order to deal with the analysis of the experimental data, it is worthwhile to select the best choice among the four density distributions of the ${}^6\text{Li}$ nucleus. Therefore, the elastic-scattering differential cross sections generated by the S1Y and M3Y interactions with four density distributions are calculated and compared with the experimental data. The volume WS imaginary three parameters shown in the tables of Refs. [27–30] are used as a starting point in my calculations. The best fit is observed for the GIT and COSMA density distributions whereas the worse for the F2P form. Hence, we chose GIT because its rms radius is compatible with the recent rms radius value determined by Tanihata *et al.* [46].

The elastic-scattering data have been analyzed using the DF potential generated by the selected ${}^6\text{Li}$ density distribution with the two effective interactions S1Y and M3Y outlined above. The four parameters, the real depth (V_0) for the S1Y interaction or renormalization factor (N_R), for the M3Y interaction in addition to the three imaginary WS parameters for each case are adjusted to fit the experimental scattering data.

Figures 1 and 2 reveal also a comparison between experimental elastic-scattering data for the seven reactions consid-

FIG. 3. Nuclear matter density distributions for the ${}^6\text{Li}$ projectile.

ered in this paper and the theoretical predictions produced

by the derived S1Y and M3Y semimicroscopic DF potentials described by the best-fit parameters listed in Table III. The solid and dotted curves show the results of the best-fit semimicroscopic DF calculations based upon the S1Y and M3Y effective interactions, respectively. All the calculated cross sections reproduce successfully the experimental data up to the most backward measured angles except for the ${}^6\text{Li} + {}^{24}\text{Mg}$ reaction with the M3Y interaction where underestimation of the data is shown at the backward angle. Chen and co-workers [27–30] investigated the same set of experimental data by using DF calculations based upon several density-dependent and density-independent NN interactions. Without the scaling factor introduced for the real potentials in their calculations, fits to the experimental elastic-scattering data cannot be achieved. It is obvious that my resulting scattering cross section with the data is on the same footing with those obtained by them. It seems that the folding model calculations for the two interested types of S1Y and M3Y effective NN interactions are valid for all targets at both forward and backward angles.

For more investigation, the notch technique [47–49] is performed to explore the sensitivity of the calculated scattering angular distributions to the radial regions of the derived real DF potentials for the considered interactions. A localized perturbation is performed into the generated real DF radial potentials. Then, the notch radially moves through the potential

TABLE III. Best-fit parameters of the semimicroscopic S1Y and M3Y potentials for scattering data.

Interaction	V_0^a	J_R (MeV fm ³)	$\langle r^2 \rangle_R^{1/2}$ (fm)	W (MeV)	r (fm)	a (fm)	J_W (MeV fm ³)	$\langle r^2 \rangle_W^{1/2}$ (fm)	σ_R (mb)	χ^2
${}^6\text{Li} + {}^{24}\text{Mg}$										
S1Y	56.93	245.35	4.13	27.56	1.062	0.904	132.05	5.12	1598	2.01
M3Y	0.671	245.94	4.12	34.54	0.955	1.079	143.08	5.31	1755	2.19
${}^6\text{Li} + {}^{28}\text{Si}$										
S1Y	60.68	261.52	4.19	32.24	1.017	0.894	128.11	5.07	1629	2.04
M3Y	0.722	264.65	4.19	32.18	1.020	0.928	131.17	5.16	1686	2.21
${}^6\text{Li} + {}^{40}\text{Ca}$										
S1Y	56.03	241.47	4.48	32.11	1.036	0.984	118.54	5.57	1991	1.68
M3Y	0.655	240.36	4.47	29.64	1.068	0.978	117.81	5.65	2021	2.12
${}^6\text{Li} + {}^{48}\text{Ca}$										
S1Y	55.90	240.92	4.53	33.34	1.032	0.922	109.28	5.54	2012	1.47
M3Y	0.648	237.59	4.52	29.96	1.072	0.890	106.96	5.61	2015	1.19
${}^6\text{Li} + {}^{58}\text{Ni}$										
S1Y	55.62	239.70	4.71	33.10	1.054	0.982	108.49	5.90	2275	2.13
M3Y	0.651	238.60	4.70	33.05	1.050	1.034	109.93	6.01	2363	1.24
${}^6\text{Li} + {}^{90}\text{Zr}$										
S1Y	57.20	246.54	5.16	31.59	1.117	0.947	100.61	6.49	2728	1.72
M3Y	0.658	241.27	5.15	31.48	1.115	0.989	101.18	6.57	2804	1.28
${}^6\text{Li} + {}^{116}\text{Sn}$										
S1Y	59.02	254.38	5.47	30.11	1.177	0.915	101.68	6.94	3060	1.16
M3Y	0.640	234.78	5.46	37.46	1.106	0.959	106.67	6.75	3037	1.41

^a $V_0 = N_R$ for M3Y calculations.

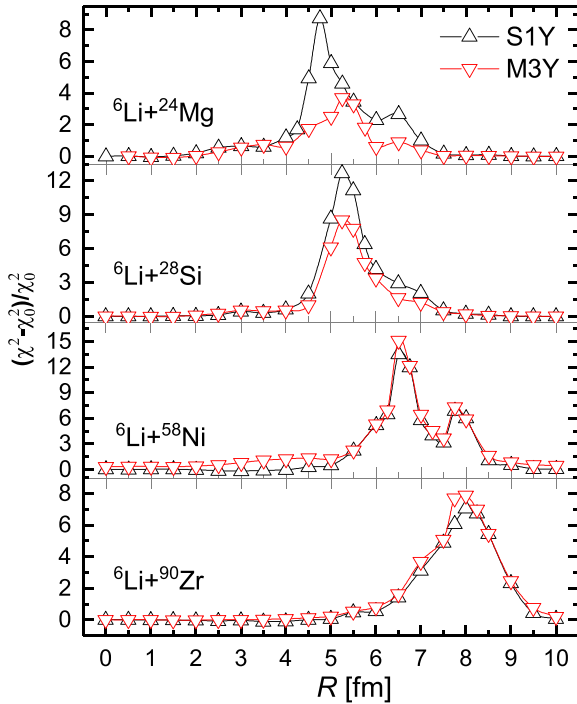


FIG. 4. Radial sensitivity of the differential cross sections of ${}^6\text{Li}$ elastic scattering from ${}^{24}\text{Mg}$, ${}^{28}\text{Si}$, ${}^{58}\text{Ni}$, and ${}^{90}\text{Zr}$ at the incident energy of 240 MeV to the semimicroscopic DF real S1Y and M3Y potentials. The curves are used to guide the eye.

to discover the influence arising from this perturbation in the resulted cross sections. Thus, the real part of the DF potentials is multiplied by factor

$$f(R; r_1, r_2, d) = 1.0 - d \exp\{-[(R - r_1)/r_2]^2\}, \quad (8)$$

where r_1 is varied from 0.0 to 10 fm in 0.5-fm steps. The other parameters, the width r_2 , and the amplitude d of the notch are taken from Ref. [49]. With the fixed perturbation parameters, the resulted ratio $\{[\chi^2(R) - \chi_0^2]/\chi_0^2\}$ versus R is used to judge the sensitivity of the scattering to the radial region as illustrated in Fig. 4. $\chi^2(R)$ and χ_0^2 , respectively, represent the resulted best-fit value corresponding to the perturbed and unperturbed DF real potentials listed in Table III. It can be seen from Fig. 4 that the peak of the greatest sensitivity lies at the surface region whereas a negligible effect is apparent in the internal region. A slow shift of the maximum of sensitivity to the nuclear surface is explicit as target mass increases. This figure shows clearly also that the same sensitive regions were determined for the resulting two DF real potentials. However, the relative sensitivity notably differed from each other for light targets rather than heavy ones. Therefore, it can be concluded that the sensitive region determined by the notch test is nearly model independent. In addition, elastic-scattering cross sections for the considered scattering reactions are sensitive to the nuclear matter distribution in the surface region. Furthermore, in analog to what Farid and Hassanain deduced in Ref. [11], the notch perturbation demonstrates that all the target nuclei appear effectively black to the ${}^6\text{Li}$ incident ions

inside the interior region of about 4 to 5 fm as the target mass increases.

It well known that the volume integral of the nuclear potential may be much better determined by the data than the potential itself [50]. The volume integral of the OP per interacting nucleon pair are determined by the relation,

$$J_{R,I} = \frac{1}{A_p A_T} \int U_{R,I}(R) R^2 dR, \quad (9)$$

where $U_{R,I}(R)$ denote the real and imaginary OP parts, respectively. Based upon nucleon-nucleus OP, Gupta and Murthy [51] suggested a linear equation for the real volume integrals resulted from the JLM interaction as

$$J_R = -C(1 + \gamma A_T^{-1/3}), \quad (10)$$

where $C = 147 \text{ MeV fm}^3$ and $\gamma = 2.0$. This formula shows that J_R is target mass dependent and is slowly decreasing as the target mass increases. On the other hand, for 210-MeV ${}^6\text{Li}$ scattering on ${}^{12}\text{C}$, ${}^{28}\text{Si}$, ${}^{40}\text{Ca}$, ${}^{58}\text{Ni}$, and ${}^{90}\text{Zr}$, Nadasen *et al.* [20] suggested that the volume integrals derived using a phenomenological WS form factor is dependent upon the target $A^{-1/3}$ in the same form as Eq. (10) but with $C = 215 \text{ MeV fm}^3$ and $\gamma \approx 0.88$ for the real part of the OP. The values of C and γ for the imaginary potentials are 45 MeV fm^3 and 5.9, respectively.

To investigate the target mass number dependence, the J_R and J_I values resulted from the generated DF potential using the S1Y and M3Y effective interactions are compared with both the relations of Gupta and Murthy [51] and Nadasen *et al.* [20] which are represented by the dotted and solid lines, respectively, in Fig. 5. Moreover, volume integrals obtained by Chen and co-workers [27–30] for the same interested interactions are also plotted in the figure for comparison. Generally, it is noted that, over all the interested target mass range, the volume integral decreases as the target mass increases. It is clear also that the values of the real volume integrals given by the S1Y and M3Y potentials are in good agreement with each other and consistent with those extracted by the work of Chen and co-workers [27–30]. Moreover, it is observed that, as the target mass increases, the resultant volume integrals deviate from Gupta and Murthy [51] prediction to the results of Nadasen *et al.* [20]. This behavior is reversed for the values of volume integrals for the real parts of the OPs obtained with the phenomenological WS form factors. As seen from the bottom of Fig. 5, the results of the imaginary volume integrals agree well with the prediction of Nadasen *et al.* [20] than the results of Chen and co-workers [27–30].

The obtained total reaction cross sections σ_R shown in Tables I and III are plotted against $A_T^{1/3}$ in Fig. 6. It is evident that the reaction cross sections have a clear linear behavior with the cubic root of the target mass number. The results obtained by using the S1Y and M3Y effective NN interactions are consistent with those obtained by Chen and co-workers [27–30] where the CDM3Y6 potentials was used. It is noted that the S1Y results are in very good agreement with those obtained by Chen and co-workers [27–30] than obtained by the M3Y results.

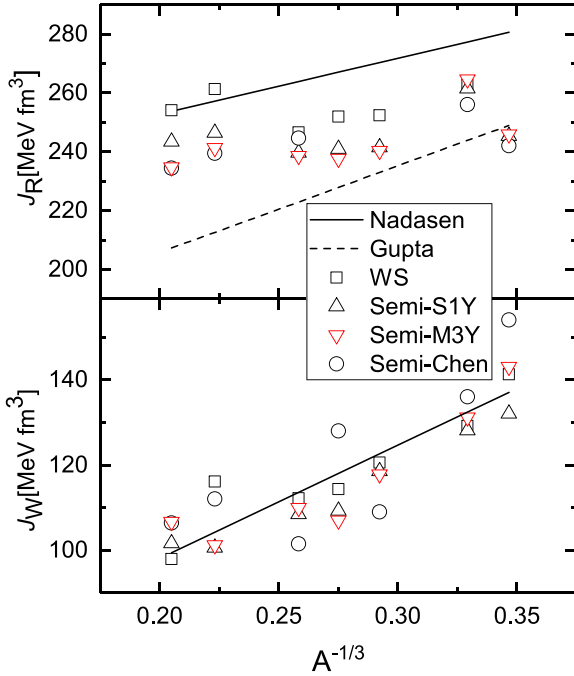


FIG. 5. The target mass number dependence of the real J_R and imaginary J_I volume integrals resulted by the S1Y and M3Y semimicroscopic potentials. The solid and dashed lines represent the expression of Nadasen *et al.* [20] obtained with WS potentials and the predictions of Gupta and Murthy [51] with microscopic JLM potentials. For comparison, volume integral obtained by Chen and co-workers [27–30] are also included.

IV. SUMMARY

Throughout this paper, the angular distributions of ${}^6\text{Li}$ elastic scattering from ${}^{24}\text{Mg}$, ${}^{28}\text{Si}$, ${}^{40}\text{Ca}$, ${}^{48}\text{Ca}$, ${}^{58}\text{Ni}$, ${}^{90}\text{Zr}$, and ${}^{116}\text{Sn}$ have been analyzed in the frame of the OM at 240 MeV. The analysis of the data has been performed in terms of phenomenological WS form factors as well as the density-independent semimicroscopic DF model. Successful reproduction of the elastic-scattering data is obtained using the volume WS form factor potentials for all considered reactions. For the DF calculations, two effective density-independent NN interactions S1Y and M3Y are used to construct the real part of the DF potential, whereas the imaginary part is taken in WS volume form. Furthermore, the experimental data are used for checking the preferable ${}^6\text{Li}$ density distribution. For this purpose, four density distributions with rms radii ranging from 2.195 to 2.444 fm are used for the ${}^6\text{Li}$ nucleus in the DF calculations. The comparison between results reveals that the G1T form with a rms radius of 2.36 fm is the best choice. The derived S1Y semimicroscopic potentials provide an excellent prediction of the data over the all measured angular ranges. Successful predictions are also obtained for M3Y potentials for all targets except the ${}^{24}\text{Mg}$ target where a little underestimation at backward angles is noted. It may be due to an additional absorption included in the imaginary potential part and because of that ${}^{24}\text{Mg}$ is strongly deformed and, hence, coupling to the 2^+ state will affect the elastic-scattering cross sections. The renormalization factor for M3Y

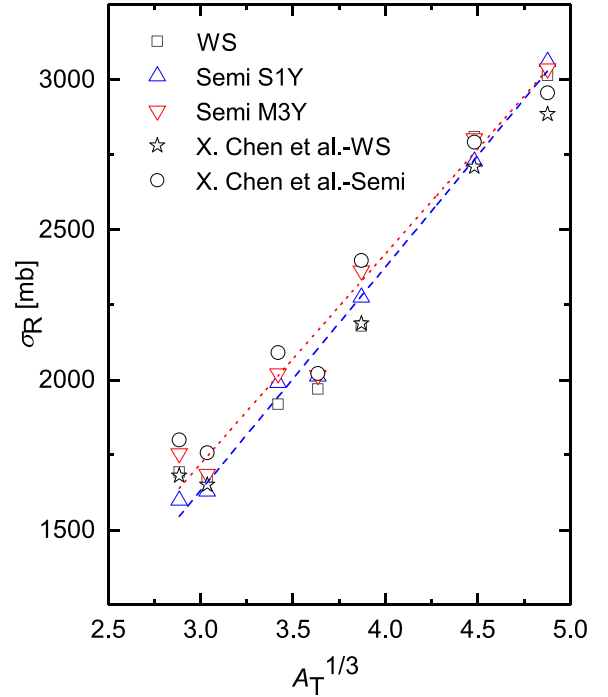


FIG. 6. The total reaction cross sections obtained by the phenomenological WS and DF calculations versus $A_T^{1/3}$ for our interested reactions. The dashed and dot lines are the least-squares fits to the results of S1Y and M3Y semimicroscopic DF calculations, respectively. The total reaction cross sections obtained by Chen and co-workers [27–30] are also included for comparison.

real OPs (0.64–0.72) is needed in order to reproduce the data where decreasing the target mass number increases the renormalization factor. This reduction in the renormalization is most probably produced by the breakup of the lithium projectile in the field of the target nucleus. The radial dependence of the resulted DF real S1Y potential is compared with that of the M3Y, and the sensitivity of the elastic-scattering cross section to the two OM potentials as a function of radius is analyzed by the notch test. Throughout the paper, it is found that the resulting semimicroscopic real volume integrals for both S1Y and M3Y potentials have approximately the same values except small differences shown for the largest two target masses. It has been observed that, as the target mass number increases, the real volume integrals for both effective interactions have a tendency from the predictions of Gupta and Murthy [51] to Nadasen *et al.* [20] except for the ${}^{28}\text{Si}$ target. Furthermore, the results of the imaginary volume integrals are spread more closely around the prediction of Nadasen *et al.* [20] than the results of Chen and co-workers [27–30]. The reaction cross sections generated from the OM calculations indicate an explicit target mass dependence. This result is quite compatible with that deduced previously [20,27–30].

The main advantage of our paper is to put forward a simple DF calculation to generate the real OP for analyzing the elastic-scattering cross sections. Although the part of the DPP which represents the breakup effect is not shown explicitly in our calculations, very good results are obtained. According to

these results, the question arises could the simple S1Y effective interaction included the DPP effect? Remember that neither the most famous density-dependent CDM3Y6 effective interaction nor those using the DPP [27–30] can successfully fit the above data with N_R equal to one. On the other hand, the study shows that including the higher-order corrections to the M3Y folding model calculations are necessary. Therefore,

this paper opens the door for the S1Y effective interaction to play an important role in analyzing such interacting nuclei. Moreover, to present another confirmation for successful S1Y predictions, S1Y density-independent DF calculations are used now to reproduce the electromagnetic $B(EL)$ values for inelastic-scattering cross sections for the studied systems.

-
- [1] G. Bertsch, J. Borysowicz, H. McManus, and W. G. Love, *Nucl. Phys. A* **284**, 399 (1977).
- [2] G. R. Satchler and W. G. Love, *Phys. Rep.* **55**, 183 (1979).
- [3] M. El-Azab Farid and G. R. Satchler, *Nucl. Phys. A* **438**, 525 (1985).
- [4] Y. Sakuragi, M. Yahiro, and M. Kamimura, *Prog. Theor. Phys. Suppl.* **89**, 136 (1986).
- [5] Y. Sakuragi, *Phys. Rev. C* **35**, 2161 (1987).
- [6] Y. Sakuragi, M. Ito, Y. Hirabayashi, and S. Chhanda, *Prog. Theor. Phys.* **98**, 521 (1997).
- [7] D. Y. Pang and R. S. Mackintosh, *Phys. Rev. C* **84**, 064611 (2011).
- [8] R. S. Mackintosh and N. Keeley, *Phys. Rev. C* **81**, 034612 (2010).
- [9] V. Lapoux *et al.*, *Phys. Lett. B* **517**, 18 (2001).
- [10] V. Lapoux, N. Alamanos, F. Auger, V. Fékou-Youmbi, A. Gillibert, F. Marie *et al.*, *Phys. Rev. C* **66**, 034608 (2002).
- [11] M. El-Azab Farid and M. A. Hassanain, *Nucl. Phys. A* **678**, 39 (2000); **697**, 183 (2002).
- [12] R. M. DeVries, D. A. Goldberg, J. W. Watson, M. S. Zisman, and J. G. Cramer, *Phys. Rev. Lett.* **39**, 450 (1977).
- [13] H. G. Bingham, M. L. Halbert, D. C. Hensley, E. Newman, K. W. Kemper and, and L. A. Charlton, *Phys. Rev. C* **11**, 1913 (1975).
- [14] J. E. Poling, E. Norbeck and, and R. R. Carlson, *Phys. Rev. C* **13**, 648 (1976).
- [15] L. T. Chua, F. D. Becchetti, J. Jänecke, and F. L. Milder, *Nucl. Phys. A* **273**, 243 (1976).
- [16] P. Schwandt, W. W. Jacobs, M. D. Kaitchuck, P. P. Singh, W. D. Ploughe, F. D. Becchetti, and J. Jänecke, *Phys. Rev. C* **24**, 1522 (1981).
- [17] S. Micek, Z. Majka, H. Rebel, H. J. Gils, and H. Klewe-Nebenius, *Nucl. Phys. A* **435**, 621 (1984).
- [18] A. C. Demijanov, V. N. Bragin, A. A. Ogloblin, A. L. Lebedev, J. M. Bang, S. A. Goncharov, S. N. Ershov, F. A. Gareev, and P. P. Korovin, *Phys. Lett. B* **184**, 129 (1987).
- [19] A. Nadasen *et al.*, *Phys. Rev. C* **37**, 132 (1988).
- [20] A. Nadasen, M. McMaster, M. Fingal, J. Tavormina, P. Schwandt, J. S. Winfield, M. F. Mohar, F. D. Becchetti, J. W. Jänecke, and R. E. Warner, *Phys. Rev. C* **39**, 536 (1989).
- [21] A. Nadasen *et al.*, *Phys. Rev. C* **47**, 674 (1993).
- [22] K. Schwarz *et al.*, *Eur. Phys. J. A* **7**, 367 (2000).
- [23] M. El-Azab Farid and M. A. Hassanain, *Eur. Phys. J. A* **19**, 231 (2004).
- [24] L. Trache, A. Azhari, H. L. Clark, C. A. Gagliardi, Y.-W. Lui, A. M. Mukhamedzhanov, R. E. Tribble, and F. Carstoiu, *Phys. Rev. C* **61**, 024612 (2000).
- [25] F. Carstoiu, L. Trache, R. E. Tribble, and C. A. Gagliardi, *Phys. Rev. C* **70**, 054610 (2004).
- [26] T. Furumoto and Y. Sakuragi, *Phys. Rev. C* **74**, 034606 (2006).
- [27] X. Chen, Y.-W. Lui, H. L. Clark, Y. Tokimoto, and D. H. Youngblood, *Phys. Rev. C* **80**, 014312 (2009).
- [28] Krishichayan, X. Chen, Y.-W. Lui, J. Button, and D. H. Youngblood, *Phys. Rev. C* **81**, 044612 (2010).
- [29] Krishichayan, X. Chen, Y.-W. Lui, Y. Tokimoto, J. Button, and D. H. Youngblood, *Phys. Rev. C* **81**, 014603 (2010).
- [30] X. Chen, Y.-W. Lui, H. L. Clark, Y. Tokimoto, and D. H. Youngblood, *Phys. Rev. C* **76**, 054606 (2007).
- [31] M. El-Azab Farid, Z. M. M. Mahmoud, and G. S. Hassan, *Nucl. Phys. A* **691**, 671 (2001); *Phys. Rev. C* **64**, 014310 (2001).
- [32] M. El-Azab Farid, *Phys. Rev. C* **65**, 067303 (2002).
- [33] M. Karakoc and I. Boztosun, *Phys. Rev. C* **73**, 047601 (2006); *Int. J. Mod. Phys. E* **15**, 1317 (2006).
- [34] M. A. Hassanain, M. Anwar, and K. O. Behairy, *Phys. Rev. C* **97**, 044610 (2018).
- [35] S. Hossain, M. N. A. Abdullah, A. S. B. Tariq, M. A. Uddin, A. K. Basak, K. M. Rusek, I. Reichstein, and F. B. Malik, *Eur. Phys. Lett.* **84**, 52001 (2008).
- [36] S. Hossain, M. N. A. Abdullah, A. K. Basak, S. K. Das, M. A. Uddin, A. S. B. Tariq, I. Reichstein, K. M. Rusek, and F. B. Malik, *Eur. Phys. J. A* **41**, 215 (2009).
- [37] N. M. Clarke (unpublished).
- [38] X. Chen, Ph.D. thesis, Texas A&M University, 2008.
- [39] G. R. Satchler, *Nucl. Phys. A* **579**, 241 (1994).
- [40] J. R. Beene, D. J. Horen, and G. R. Satchler, *Phys. Lett. B* **344**, 67 (1995); *Nucl. Phys. A* **596**, 137 (1996).
- [41] M. El-Azab Farid, *Phys. Rev. C* **74**, 064616 (2006).
- [42] P. J. Karol, *Phys. Rev. C* **11**, 1203 (1975).
- [43] M. Pignanelli, S. Micheletti, R. De Leo, S. Brandenburg, and M. N. Harakeh, *Phys. Rev. C* **33**, 40 (1986).
- [44] G. Fricke, C. Bernhardt, K. Heilig, L. A. Schaller, L. Schellenberg, E. B. Shera, and C. W. De Jager, *At. Data Nucl. Data Tables* **60**, 177 (1995).
- [45] D. T. Khoa and G. R. Satchler, *Nucl. Phys. A* **668**, 3 (2000).
- [46] I. Tanihata, H. Savajols, and R. Kanungo, *Prog. Part. Nucl. Phys.* **68**, 215 (2013).
- [47] J. G. Cramer and R. M. DeVries, *Phys. Rev. C* **22**, 91 (1980).
- [48] P. J. Moffa, C. B. Dover, and J. P. Vary, *Phys. Rev. C* **13**, 147 (1976).
- [49] F. Michel, J. Albinski, P. Belery, Th. Delbar, Gh. Grégoire, B. Tasiaux, and G. Reidemeister, *Phys. Rev. C* **28**, 1904 (1983).
- [50] G. R. Satchler, *Direct Nuclear Reactions* (Oxford University Press, Oxford, 1983).
- [51] S. Gupta and K. Murthy, *Z. Phys. A: Atoms Nuclei* **307**, 187 (1982).